J|A|C|S
ARTICLES

Published on Web 11/24/2009

A General Strategy for Preparation of Pt 3d-Transition Metal (Co, Fe, Ni) Nanocubes

Jun Zhang and Jiye Fang*

Department of Chemistry, State University of New York at Binghamton, Binghamton, New York 13902

Received October 5, 2009; E-mail: jfang@binghamton.edu

Abstract: A facile, reliable, general, and robust synthetic method for preparation of high-quality, (100)-terminated Pt_3M nanocubes (M = Pt or 3d-transition metals Co, Fe, and Ni) has been developed. It was identified that addition of $W(CO)_6$ is crucial for control of the nucleation process when the metallic precursors are reduced, whereas an optimized ratio of the solvent pair, oleylamine and oleic acid, is the key to enabling the lowest total surface energy on {100} facets in order to develop cubic nanocrystals in the present system. The resultant monodisperse nanocubes, in which Pt is partially substituted, are expected to exhibit unusual electrocatalytic characteristics, providing an alternative for developing high-performance electrocatalysts for use in fuel cells.

Introduction

The precious metal platinum is traditionally used as a high-performance electrocatalyst for proton-exchange membrane fuel cells and fine chemical synthesis.[1] Due to the high cost and the scarcity of Pt, it is an urgent task to develop substitutes for the pure Pt catalyst. To date, one of the most successful alternatives has involved partially substituting Pt using less expensive 3d-transition metals.[1−8] It has also been recognized that the shape and surface structure of nanocrystals (NCs) play significant roles in electrocatalytic activity[9−11] and reaction durability.[4,12] For instance, it has been reported that cubic Pt NCs possess unusual catalytic activity in oxidation reactions.[1,13] As is well-known, the electron density of states is actually sensitive to the surface structure, and different crystal facets could have diverse catalytic natures. In order to enhance catalytic performance while minimizing the use of precious metal Pt, it is worthwhile to prepare various shape-controlled nano-polyhedra containing Pt and 3d-transition metals, such as {100}-terminated nanocubes and {111}-bounded nano-octohedra, and to experimentally survey the catalytic characteristics of various crystal facets on each binary alloy. Unfortunately, there is still no general strategy to fabricate shape-controlled nano-polyhedra of Pt-based alloys, although syntheses of pure Pt[1,14−16] and PtFe[17] nanocubes (NCbs) have recently been demonstrated.

In this article, we report a novel, robust, and general approach to the synthesis of monodisperse and high-yield NCbs of Pt and Pt-based binary alloys containing a relatively broad spectrum of 3d-tranistion metals. The unique aspects of this new synthetic strategy are the control of both the nucleation process and the subsequent crystal growth stage by using tungsten hexacarbonyl [$W(CO)_6$] and the ability to tune the total surface energies on various crystal facets in solution by altering their binding-agent capability (*vide infra*). Specifically, reduction of platinum(II) acetylacetonate [$Pt(acac)_2$] produces Pt NCbs, whereas co-reduction of $Pt(acac)_2$ and a metal salt (M = Co, Fe, or Ni)—that is, cobalt acetate tetrahydrate ($CoAc_2 \cdot 4H_2O$), iron(II) chloride tetrahydride ($FeCl_2 \cdot 4H_2O$), or nickel(II) chloride hexahydride ($NiCl_2 \cdot 6H_2O$)—generates Pt_3Co, Pt_3Fe, or Pt_3Ni NCbs.

Experimental Section

NCbs of Pt_3M (M = Pt, Co, Fe, and Ni) were systematically prepared through a general approach in which a co-reduction of platinum(II) acetylacetonate [$Pt(acac)_2$] and M-salt in a mixed

(1) Wang, C.; Daimon, H.; Lee, Y.; Kim, J.; Sun, S. *J. Am. Chem. Soc.* **2007**, *129*, 6974–6975.
(2) Paulus, U. A.; Wokaun, A.; Scherer, G. G.; Schmidt, T. J.; Stamenkovic, V.; Markovic, N. M.; Ross, P. N. *Electrochim. Acta* **2002**, *47*, 3787–3798.
(3) Stamenkovic, V.; Mun, B. S.; Mayrhofer, K. J. J.; Ross, P. N.; Markovic, N.; Rossmeisl, J.; Greeley, J.; Nørskov, J. K. *Angew. Chem., Int. Ed.* **2006**, *45*, 2897–2901.
(4) Stamenkovic, V. R.; Mun, B. S.; Arenz, M.; Mayrhofer, K. J. J.; Lucas, C. A.; Wang, G.; Ross, P. N.; Markovic, N. M. *Nat. Mater.* **2007**, *6*, 241–247.
(5) Mukerjee, S.; Srinivasan, S.; Soriaga, M. P. *J. Electrochem. Soc.* **1995**, *142*, 1409–1422.
(6) Watanabe, M.; Tsurumi, K.; Mizukami, T.; Nakamura, T.; Stonehart, P. *J. Electrochem. Soc.* **1994**, *141*, 2659–2668.
(7) Koh, S.; Leisch, J.; Toney, M. F.; Strasser, P. *J. Phys. Chem. C* **2007**, *111*, 3744–3752.
(8) Shevchenko, E. V.; Talapin, D. V.; Schnablegger, H.; Kornowski, A.; Festin, ö.; Svedlindh, P.; Haase, M.; Weller, H. *J. Am. Chem. Soc.* **2003**, *125*, 9090–9101.
(9) Narayanan, R.; El-Sayed, M. A. *J. Am. Chem. Soc.* **2004**, *126*, 7194–7195.
(10) Narayanan, R.; El-Sayed, M. A. *Nano. Lett.* **2004**, *4*, 1343–1348.
(11) Tian, N.; Zhou, Z.-Y.; Sun, S.-G.; Ding, Y.; Wang, Z. L. *Science* **2007**, *316*, 732–735.
(12) Peng, Z.; Yang, H. *Nanotoday* **2009**, *4*, 143–164.
(13) Wang, C.; Daimon, H.; Onodera, T.; Koda, T.; Sun, S. *Angew. Chem., Int. Ed.* **2008**, *47*, 3588–3591.
(14) Kim, C.; Lee, H. *Catal. Commun.* **2009**, *10*, 1305–1309.
(15) Habas, S. E.; Lee, H.; Radmilovic, V.; Somorjai, G. A.; Yang, P. *Nat. Mater.* **2007**, *6*, 692–697.
(16) Lee, H.; Habas, S. E.; Kweskin, S.; Butcher, D.; Somorjai, G. A.; Yang, P. *Angew. Chem., Int. Ed.* **2006**, *45*, 7824–7828.
(17) Chen, M.; Kim, J.; Liu, J. P.; Fan, H.; Sun, S. *J. Am. Chem. Soc.* **2006**, *128*, 7132–7133.

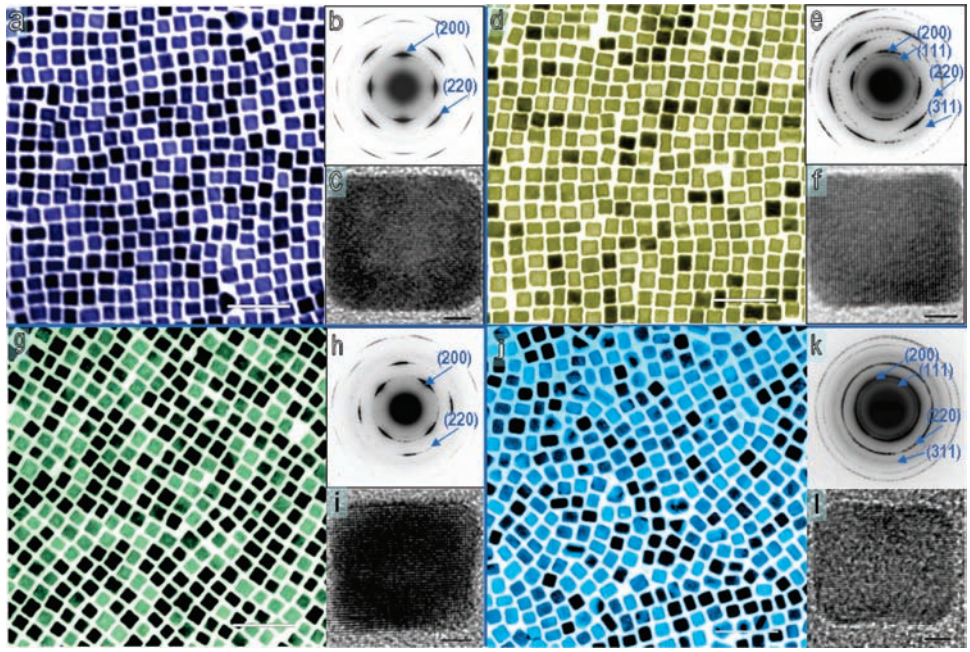

Figure 1. TEM images and diffraction patterns: (a−c) Pt nanocubes; (d−f) Pt_3Co nanocubes; (g−i) Pt_3Fe nanocubes; and (j−l) Pt_3Ni nanocubes. Panels a, d, g, and j show TEM images (data bars represent 50 nm); b, e, h, and k show the selected area electron diffraction (negative) patterns of the nanocubes; and c, f, i, and l show high-resolution TEM images of the nanocubes (scale bars represent 2 nm). Synthesis conditions are described in the Experimental Section.

organic solvent of oleic acid and oleylamine was carried out at around 240 °C. The synthesis is described in detail as follows.

Chemicals. Cobalt(II) acetate tetrahydrate (99.999%), iron(II) chloride tetrahydrate (99.99%), tungsten hexacarbonyl (97%), benzyl ether (99%), oleic acid (90%), and oleylamine (70%) are Aldrich products. Nickel(II) chloride hexahydrate (96+%) was received from Fisher Scientific. Platinum(II) acetylacetonate (49.3−49.8% Pt), anhydrous ethanol (200 proof), and anhydrous hexane (98.5%) were purchased from Gelest, AAPER, and BDH, respectively. All chemicals were used without further purification.

Characterization Method. X-ray diffraction patterns were collected using a PANalytical X'Pert X-ray powder diffractometer equipped with a Cu $K\alpha_1$ radiation source ($\lambda = 0.15406$ nm). A Hitachi 7000 transmission electron microscope (TEM) operated at 110 kV was used for traditional TEM imaging, and a JEOL-2010 FEG TEM operated at 200 kV was used for high-resolution TEM imaging, selected-area electron diffraction (SAED), and energy-dispersive X-ray spectroscopy data collection. ICP-MS and ICP-AES analyses were conducted at the Department of Geosciences, University of Houston. Infrared spectra were acquired using a Bruker FTIR spectrometer (EQUINOX 55). X-ray photoelectron spectroscopy (XPS) analysis was conducted on a Surface Science Instruments SSX-100 with an operating pressure of $<2 \times 10^{-9}$ Torr and monochromatic Al Kα X-rays at 1486.6 eV. Beam diameter was 1000 μm. Photoelectrons were collected at an emission angle of 55° from the surface normal hemispherical analyzer with pass energy of 150 V for survey scans and 50 V for high-resolution scans.

Synthesis Details. 1. Synthesis of Pt NCbs. A 0.020 g sample of platinum(II) acetylacetonate, 8.0 mL of oleylamine, and 2.0 mL of oleic acid were loaded into a three-neck flask equipped with a condenser and attached to a Schlenk line. The mixture was heated to 130 °C with vigorous stirring under an argon stream. Next, 0.05 g of tungsten hexacarbonyl was added into the solution, and the temperature was subsequently raised to 240 °C and kept for 30−60 min with vigorous agitation. The resultant products were isolated by centrifugation and washed with anhydrous hexane for several cycles, followed by a size-selection treatment. The Pt NCbs were finally redispersed in hexane, forming a colloidal suspension.

2. Synthesis of Pt_3Co NCbs. A 0.0125 g sample of cobalt acetate tetrahydrate, 0.020 g of platinum(II) acetylacetonate, 8.0 mL of oleylamine, and 2.0 mL of oleic acid were loaded into a three-neck flask equipped with a condenser and attached to a Schlenk line. The mixture was heated to 130 °C with vigorous stirring under an argon stream. Next, 0.05 g of tungsten hexacarbonyl was added into the solution, and the temperature was subsequently raised to 240 °C and kept for 30−60 min with vigorous agitation. The isolation procedure is the same as above.

3. Synthesis of Pt_3Fe NCbs. A 0.010 g sample of iron(II) chloride tetrahydrate, 0.020 g of platinum(II) acetylacetonate, 8.0 mL of oleylamine, and 2.0 mL of oleic acid were loaded into a three-neck flask equipped with a condenser and attached to a Schlenk line. The mixture was heated to 130 °C with vigorous stirring under an argon stream. Next, 0.05 g of tungsten hexacarbonyl was added into the solution, and the temperature was subsequently raised to 240 °C and kept for 30−60 min with vigorous agitation. The isolation procedure is the same as that described for Pt NCbs.

4. Synthesis of Pt_3Ni NCbs. Under airless conditions, platinum(II) acetylacetonate (0.020 g, 0.05 mmol), oleylamine (8.0 mL), and oleic acid (2.0 mL) were loaded into a three-neck flask under an argon stream. Once the system was heated to 130 °C, tungsten hexacarbonyl (0.050 g, 0.14 mmol) was added into the vigorously stirred solution. Subsequently, a stock solution of Ni precursors (0.4 mL, 0.04 mmol), which was pre-prepared by dissolving 0.238 g of nickel(II) chloride hexahydride into mixed solvents containing oleylamine (5.0 mL) and oleic acid (5.0 mL), was added dropwise within 15 min while the temperature was steadily raised from 130 to 200 °C. The colloids were further evolved at 240 °C for an additional 15 min. The isolation procedure is the same as that described for Pt NCbs.

Results and Discussion

Typical TEM images of the four types of NCbs are presented in Figure 1. Panels a, d, g, and j show a perfect cubic morphology for each system and relatively high size distribution (also refer to Figure 2). On the basis of the TEM images of these Pt, Pt_3Co, Pt_3Fe, and Pt_3Ni NCbs, average side-lengths

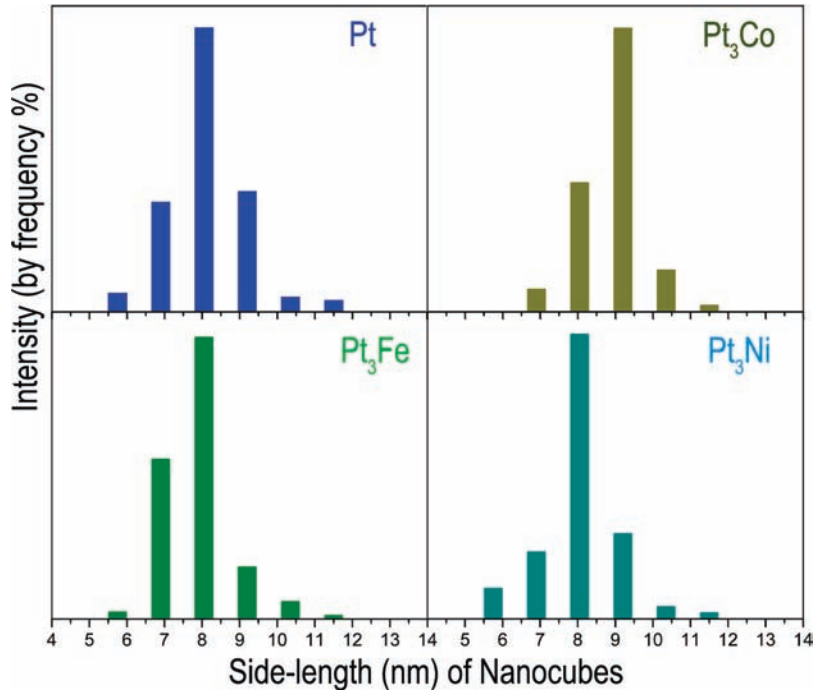

Figure 2. Particle size (side-length) distribution of four types of nanocubes: Pt, Pt_3Co, Pt_3Fe, and Pt_3Ni. Data are from TEM images of more than 200 selected particles in each case.

were determined as 8.1 ± 0.6, 9.1 ± 0.5, 7.9 ± 0.6, and 8.1 ± 0.6 nm, respectively. As depicted in Figure 1, each of panels b, e, h, and k, SAED (negative) patterns of these NCbs, were taken from about 150−200 NCs. The ring corresponding to the (200) plane in the SAED patterns of Pt, Pt_3Co, Pt_3Fe, and Pt_3Ni exhibits four-fold symmetry, clearly indicating that these NC arrays are (100)-textured with a relatively long-range order. This observation is also supported by the facts that the (111) diffraction rings are very weak and the (222) rings are absent in the case of all four types of NCbs. Panels c, f, i, and l in Figure 1 present high-resolution TEM (HRTEM) images of individual NCbs in each case (also see Figure S1, Supporting Information), indicating highly crystalline cubes with apparently resolved lattice fringes. The measured *d*-spacings, that is, 1.96, 1.92, 1.93, and 1.94 Å, are consistent with {200} for Pt, Pt_3Co, and Pt_3Fe lattice planes[18] and literature reports for Pt_3Ni,[19,20] respectively. This not only reveals that these NCbs are perfectly (100)-oriented but also indirectly verifies the compositions of Pt−Co and Pt−Fe. In addition, no distortion of the crystal cores was observed from these HRTEM images (see Figure S1). To explore the chemical compositions, typical samples of these binary alloys were analyzed using TEM energy-dispersive X-ray spectroscopy (TEM-EDS), and the outcomes were generally in good agreement with our inductively coupled plasma mass spectroscopic (ICP-MS) and inductively coupled plasma atomic emission spectrophotometric (ICP-AES) results. As presented in Figure S2 (Supporting Information), the EDS evaluation suggests that the average molar ratios between Pt and M in three binary alloys are close to 3:1. We have also investigated the influence of the Pt/M precursor ratios on the composition of the products. It seems that the compositions of NCbs can be changed slightly by varying the feed ratios between the Pt and M precursors; however, the influence is insignificant. For example, increasing the (Fe) input molar ratio of Fe/Pt from 1:1 to 2:1 only increased the (Fe) molar ratio of Fe/Pt from 22.3:77.7 to 24.0:76.0 in the cubic products when the synthesis was carried out at 240 °C.

To further confirm the microstructure of these NCbs, X-ray diffraction (XRD) patterns were recorded from all of the Pt_3M samples; they are presented in Figure 3a−d. By indexing these XRD patterns using standard ICDD PDF cards[18] and reported data,[19,20] it is confirmed that the as-synthesized NCbs possess a highly crystalline face-centered cubic Pt phase with the $Fm\bar{3}m$ space group. Importantly, no diffraction signal of pure M and/or pure W was detected from all of the patterns, further indicating that only a single Pt_3M phase exists in each sample. It is worth noting that when these NCbs were carefully deposited on a surface-polished Si wafer, as reported previously,[1,21,22] the resultant XRD pattern of each sample showed a greatly enhanced (200) peak (Figure 3e−h), indicating that these Pt_3M NCbs align perfectly flat on the surface of the substrates with (100) texture. In comparison with the XRD patterns of the same Pt_3M cubic samples randomly deposited on a regular XRD holder/substrate (Figure 3a−d), this enhancement of the (200) peak in the XRD observation further supports that the Pt_3M NCbs have a {100}-dominated cubic morphology with very narrow shape distributions.

It is broadly accepted that the evolution of NCs in a solution system consists of a nucleation stage and a subsequent Ostwald ripening growth on the existing seeds (or nuclei).[23,24] As shown in Scheme 1, the rates of nucleation and subsequent NC growth

(18) Refer to JCPDS-ICDD cards: Pt, 04-0802; Pt_3Co, 29-0499; Pt_3Fe, 89-2050, 29-0716, and 29-1423.
(19) Ahrenstorf, K.; Heller, H.; Kornowski, A.; Broekaert, J. A. C.; Weller, H. *Adv. Funct. Mater.* **2008**, *18*, 3850–3856.
(20) Ahrenstorf, K.; Albrecht, O.; Heller, H.; Kornowski, A.; Gçrlitz, D.; Weller, H. *Small* **2007**, *3*, 271–274.
(21) Lu, W.; Fang, J.; Stokes, K. L.; Lin, J. *J. Am. Chem. Soc.* **2004**, *126*, 11798–11799.
(22) Zhang, J.; Kumbhar, A.; He, J.; Das, N. C.; Yang, K.; Wang, J.-Q.; Wang, H.; Stokes, K. L.; Fang, J. *J. Am. Chem. Soc.* **2008**, *130*, 15203–15209.
(23) Xiong, Y.; Xia, Y. *Adv. Mater.* **2007**, *19*, 3385–3391.

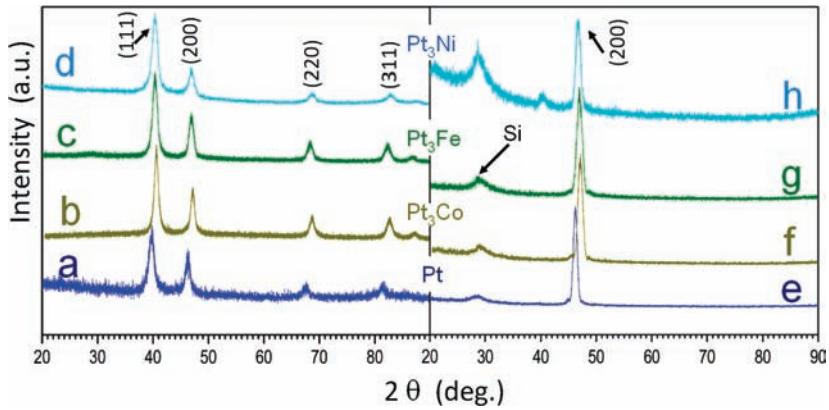

Figure 3. XRD pattern of Pt_3M nanocubes: (a,e) Pt, (b,f) Pt_3Co, (c,g) Pt_3Fe, and (d,h) Pt_3Ni. (a−d) Samples were randomly deposited on a PANalytical zero-background Si sample holder. (e−h) Samples were assembled on a surface-polished 25 mm Si ⟨100⟩ wafer.

Scheme 1. Illustration of Both Nucleation and Crystal Growth Processes for Pt_3M Nanocubes (M = Co, Fe, and Ni)

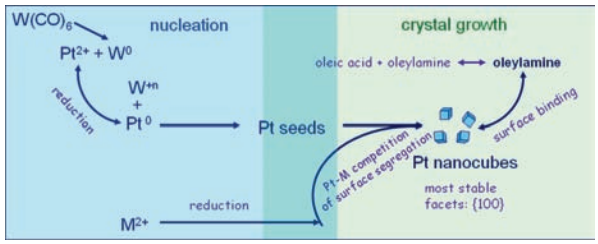

are the keys to shape control.[23,25] Ideally, a large number of critical nuclei should be formed in a short interval of time, followed by the simultaneous and steady growth of those nuclei.[26] A relatively slow rate of crystal growth usually results in growth much more selectively in crystal directions and benefits the shape control of NCs.[27] However, the short nucleation burst often consumes most precursors, resulting in less shape-controlled colloids because there is insufficient feedstock for the growth stage.[24] To circumvent this, we chose to control the nucleation process in order to provide a constant feedstock for stable subsequent Ostwald ripening growth by introducing a foreign element, tungsten. Since W does not alloy with Pt under the reaction conditions[28−30] (which is supported by the results of ICP-MS/AES and EDS analyses), we propose that the relatively low redox potential of W decomposed from $W(CO)_6$, in comparison with that of Pt,[31] could help reduce $Pt(acac)_2$ to Pt atoms (or seeds) rapidly in the early stage of the nucleation, leading to a fast Pt reduction. The resultant W cations may accumulate in a relatively high concentration that will decelerate the subsequent metallic particle growth under the following equilibrium:

$$Pt^{2+} + W^0 \rightleftharpoons W^{n+} + Pt^0$$

Thus, the Pt precursor−W system acts as a "buffer", ensuring a steady growth of particles with a sufficient feedstock. The "slowdown" of Pt nucleation favors the evolution of Pt_3M NCs because Pt clusters can be steadily and continuously provided for the Ostwald growth in this case. An additional piece of evidence supporting this notion is the observation of a W^{6+} peak in the X-ray photoelectron spectra of the reaction residue. The two observed peaks are assigned to ionic $W_{4f5/2}$ and $W_{4f7/2}$,[32] as shown in Figure S3 (Supporting Information), and no peak from W^0 was found. In another set of blank experiments, we attempted to prepare pure W NCs by decomposition of tungsten carbonyl alone under reaction conditions similar to those used for the Pt_3M preparation. However, we obtained only a transparent solution with no trace of crystalline material. It is important to report that the use of $W(CO)_6$ is essential to the success of Pt_3M NCb preparation. In the absence of $W(CO)_6$, no cubic NC formed under otherwise the same experimental conditions, as demonstrated in Figure S4 (Supporting Information). In addition, $W(CO)_6$ is not very volatile, compared to other carbonyls, such as $Fe(CO)_5$, that have been used in Pt and Pt-based alloy NC syntheses, making it safer and easier to control the input amount.

It is also commonly believed that the tiny nanocrystallites freshly formed after the nucleation process should be polyhedral, containing various crystallographic planes on their surfaces.[23,33] A high-surface-energy facet on a particle is an unstable plane and is associated with a high growth rate in a direction perpendicular to the facet, resulting in a rapid area-reduction or even elimination of this facet.[11,34,35] Although surface energy is an intrinsic property of a crystal facet, in a solution-based evolution environment it could be tuned with a number of parameters, including the surfactant-binding ability.[23] To facilitate the growth of Pt_3M NCs into cubes in an organic solution system, our strategy is to ensure that the {100} crystal facets have the lowest total surface energy. This promotes a rapid elimination of other Pt_3M planes, leading to the formation of Pt_3M NCbs. It was reported that addition of oleic acid and oleylamine in sequence could generate FePt NCbs.[17] We accordingly shared this insight and employed a mixture of oleylamine and oleic acid as a pair of solvent/reducing and binding agents in our system. It was determined that neither oleylamine nor oleic acid alone would lead to formation of the Pt_3M NCbs. It was further optimized that a ratio of 4:1 (vol%)

(24) Murray, C. B.; Kagan, C. R.; Bawendi, M. G. *Annu. Rev. Mater. Sci.* **2000**, *30*, 545–610.
(25) Zhang, J.; Sun, K.; Kumbhar, A.; Fang, J. *J. Phys. Chem. C* **2008**, *112*, 5454–5458.
(26) Sun, S.; Murray, C. B. *J. Appl. Phys.* **1999**, *85*, 4325–4330.
(27) Song, Q.; Zhang, Z. J. *J. Am. Chem. Soc.* **2004**, *126*, 6164–6168.
(28) Xiong, L.; He, T. *Electrochem. Commun.* **2006**, *8*, 1671–1676.
(29) Alexeev, O.; Shelef, M.; Gates, B. C. *J. Catal.* **1996**, *164*, 1–15.
(30) Mietrach, D. U.S. Patent 4,674,675, sheet 676/677, June 23, 1987.
(31) Vanysek, P. In *CRC Handbook of Chemistry and Physics*; Lide, D. R., Ed.; CRC Press: Boca Raton, FL, 2006; Vol. 87, pp 8/20−28/29.
(32) Bigey, C.; Logie, V.; Bensaddik, A.; Schmitt, J. L.; Maire, G. *J. Phys. IV France* **1998**, *8*, Pr5-553-560.
(33) Wang, Z. L. *J. Phys. Chem. B* **2000**, *104*, 1153–1175.
(34) Lee, S.-M.; Jun, Y.-w.; Cho, S.-N.; Cheon, J. *J. Am. Chem. Soc.* **2002**, *124*, 11244–11245.
(35) Ren, J.; Tilley, R. D. *J. Am. Chem. Soc.* **2007**, *129*, 3287–3291.

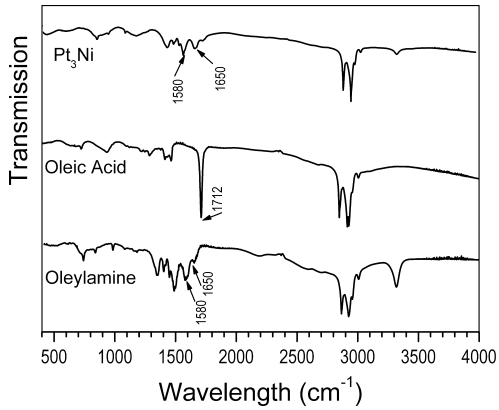

Figure 4. Fourier transform infrared spectra of as-synthesized Pt_3Ni nanocubes, oleic acid, and oleylamine.

between oleylamine and oleic acid can achieve well-defined Pt_3M NCbs (taking the case of Pt_3Co as an example, see Figure S5, Supporting Information). In addition, we found that a solvent pair of oleylamine and oleic acid is indispensable; for instance, it cannot be either partially or fully replaced by a non-coordination solvent such as dioctyl ether. To differentiate the capping agent from the stabilizing agent—that is, which one chemically caps on the surface of Pt_3M and which one temporally stabilizes the Pt_3M colloids, Fourier transform infrared (FT-IR) spectra of the as-prepared Pt_3M NCbs were collected.

As an example, Figure 4 shows a FT-IR spectrum of the as-prepared Pt_3Ni NCbs coated with the organic species, providing qualitative information about molecules capped on the surface of these NCbs. For comparison, spectra of as-used oleylamine and oleic acid are also included, which are in good agreement with the literature data.[36,37] The spectrum recorded on Pt_3Ni NCbs is similar to that of the oleylamine but not the oleic acid. For example, a band at $\sim$1712 cm^{-1} of oleic acid that can be attributed to the carbonyl C═O stretching mode[38] and a band at $\sim$1560 from the asymmetric stretching of carbonyl in oleic acid[39] are not observed in the spectrum of Pt_3Ni NCbs, whereas bands at $\sim$1580 and 1650 cm^{-1} that are assigned to the N−H deformation vibration of a primary amine[40] appear in spectra of both the oleylamine and the NCbs. These observations suggest that the organic residues finally capped on Pt_3Ni NCbs are only oleylamine, although both oleylamine and oleic acid were used in the synthesis. One more observation supporting this conclusion is that addition of oleylamine can cease aggregation of newly prepared Pt_3Ni NCs, whereas oleic acid cannot. On the basis of the above discussion, it is believed that oleylamine may act as a capping agent on metal surface sites, slowing but not stopping NC's growth. During crystal growth in solution, shape development of a NC is actually dependent on the competitive growth rates perpendicular to various surface facets. The growth rate can be determined by the total surface energy, to which the binding energy between a ligand and a given crystal facet makes a contribution. Obviously, a surface-selective capping agent may alter the morphology of a NC. We believe that oleylamine offers such a function by lowering the binding energy (and therefore total surface energy) on {100} of Pt_3M. As for the co-reducing agent in the present system, our further investigation indicates that both oleylamine and $W(CO)_6$, which subsequently generates metallic W and CO, contribute the reducing activities.

It is worth mentioning that the competitive segregation between Pt and M on the surface of a freshly resultant NC should also be an important consideration when preparing NCbs. In the case of Pt_3Ni, the addition of Ni precursors has to be postponed due to the strong alloying between Pt and Ni. Because of the lack of stoichiometric nickel precursors in this approach, Pt seeds at the initial stage as well as Pt-surface-enriched Pt_3Ni NCs in the subsequent steps should always dominate the crystal growth, which is the driving force for developing cubic NCs. On the other hand, the extremely strong ability of Ni to alloy with Pt enables the limited amount of Ni, reduced from the slowly titrated nickel precursors, to promptly combine with Pt through interlayer diffusions without formation of a pristine Ni phase nor a Pt-core/Ni-shell structure. Our investigation shows that pure Ni NCs could be detected only when the nickel precursors were introduced at a temperature higher than 210 °C.

Conclusions

In conclusion, we demonstrate a facile, reliable, and general synthetic protocol to fabricate high-quality {100}-bounded NCbs containing Pt and a 3d-transition metal, Co, Fe, or Ni. A reasonable growth mechanism for these NCbs is proposed, supported by various characterizations including XRD, EDS, XPS, and FT-IR. It was identified that the use of $W(CO)_6$ is crucial for controlling the nucleation process, whereas an optimized ratio of oleylamine and oleic acid pair is the key to enable the lowest total surface energy on {100} facets in order to develop these NCbs in the present system. These resultant monodisperse NCbs are expected to exhibit unusual electrocatalytic characteristics, providing a new opportunity for developing high-performance Pt-substituted electrocatalysts.

Acknowledgment. This work was partially supported by NSF CAREER program (DMR-0731382), the S^3IP, and Binghamton University. J.Z. thanks Zhaoyong Sun for providing the FTIR data.

Note Added after ASAP Publication. In the Experimental Section, the name for nickel(II) chloride hexahydrate was incorrect due to a production error in the version published on the web November 24, 2009. This has been corrected for the version published December 1, 2009.

Supporting Information Available: High-resolution TEM images of nanocubes; spectra of TEM-EDS analysis results; XPS spectrum of the residual solution after Pt_3Fe nanocube synthesis; TEM images when the ratio of oleylamine/oleic acid was varied and in the absence of $W(CO)_6$. This material is available free of charge via the Internet at http://pubs.acs.org.

JA908245R

(36) Yang, H. T.; Shen, C. M.; Wang, Y. G.; Su, Y. K.; Yang, T. Z.; Gao, H. J. *Nanotechnology* **2004**, *15*, 70–74.
(37) Xu, Z.; Shen, C.; Hou, Y.; Gao, H.; Sun, S. *Chem. Mater.* **2009**, *21*, 1778–1780.
(38) Roonasi, P.; Holmgren, A. *Appl. Surf. Sci.* **2009**, *255*, 5891–5895.
(39) Luo, J.; Han, L.; Kariuki, N. N.; Wang, L.; Mott, D.; Zhong, C.-J.; He, T. *Chem. Mater.* **2005**, *17*, 5282–5290.
(40) Socrates, G. *Infrared Characteristic Group Frequencies*, 2nd ed.; John Wiley & Sons: Chichester, 1994.